

## Article

# Leaching of Sulfadiazine and Florfenicol in an Entisol of a Chicken-Raising Orchard: Impact of Manure-Derived Dissolved Organic Matter

Lanre Anthony Gbadegesin <sup>1,2</sup> , Xinyu Liu <sup>1,3</sup>, Xiangyu Tang <sup>1</sup>, Chen Liu <sup>1,\*</sup> and Junfang Cui <sup>1,\*</sup> 

<sup>1</sup> Key Laboratory of Mountain Surface Processes and Ecological Regulation, Institute of Mountain Hazards and Environment, Chinese Academy of Sciences, Chengdu 610041, China

<sup>2</sup> International College, University of Chinese Academy of Sciences, Beijing 100049, China

<sup>3</sup> Faculty of Geosciences and Environmental Engineering, Southwest Jiaotong University, Chengdu 611756, China

\* Correspondence: chen1017@imde.ac.cn (C.L.); jfcui@imde.ac.cn (J.C.)

**Abstract:** Antibiotic pollution from manured farmland soils is a major public concern, and their potential interaction with manure particles and/or manure–dissolved organic matter (DOM) often complicates their leaching behaviour. This study investigated the leaching of sulfadiazine (SDZ) and florfenicol (FFC) with manure–DOM in undisturbed field lysimeters and repacked soil columns under natural and simulated rainfall conditions. The results showed that manure–DOM reduced SDZ mass flux, but soil hydrological processes and heavy rainfall events led to accelerated leaching. FFC was more prone to leaching in a manured plot ( $0.48 \mu\text{g m}^{-2} \text{h}^{-1}$ ) compared to the control ( $0.12 \mu\text{g m}^{-2} \text{h}^{-1}$ ), suggesting DOM facilitated transport of FFC in the field lysimeter study via cotransport mechanisms favored by abundant macropores in the study site. In contrast, SDZ and FFC mobility were reduced in repacked soil columns under manure–DOM conditions, suggesting complexation and adsorption in matrix pores. Two kinetic site models and two-site nonequilibrium adsorption models revealed the existence of nonequilibrium conditions and kinetic sorption processes in the repacked column. FFC exhibited lower leaching potential compared to SDZ in both the repacked column and natural field conditions. Redundancy analyses revealed that FFC had a close relationship with humic-like components (C1 and C3), but SDZ was more related to the protein-like components (C2) of DOM. The presence of manure–DOM may decrease the ecological risks of highly mobile antibiotics under matrix flow through complexations and adsorption. However, a similar scenario in macroporous flow under heavy rainfalls may lead to accelerated leaching.

**Keywords:** antibiotics; leaching; mass flux; manure; EEM-PARAFAC; farmland



**Citation:** Gbadegesin, L.A.; Liu, X.; Tang, X.; Liu, C.; Cui, J. Leaching of Sulfadiazine and Florfenicol in an Entisol of a Chicken-Raising Orchard: Impact of Manure-Derived Dissolved Organic Matter. *Agronomy* **2022**, *12*, 3228. <https://doi.org/10.3390/agronomy12123228>

Academic Editor: Yolanda Martínez Martínez

Received: 22 November 2022

Accepted: 15 December 2022

Published: 19 December 2022

**Publisher's Note:** MDPI stays neutral with regard to jurisdictional claims in published maps and institutional affiliations.



**Copyright:** © 2022 by the authors. Licensee MDPI, Basel, Switzerland. This article is an open access article distributed under the terms and conditions of the Creative Commons Attribution (CC BY) license (<https://creativecommons.org/licenses/by/4.0/>).

## 1. Introduction

Veterinary antibiotics are widely used in animal husbandry to treat diseases and promote livestock productivity. Globally, China is the largest producer and user of veterinary antibiotics [1,2], and a large proportion are used in swine, cattle and poultry production [3,4]. Recently, it was suggested that the growth rate of poultry meat production in China may exceed pork production, with 18.9 Mt of poultry meat produced in 2016 and an average 7.2% annual increase in egg production [5]. Thus, antibiotics used for chicken production are predicted to increase by 143% from 2010 to 2030 [1]. The main concern over extensive consumption is that veterinary antibiotics are not entirely adsorbed or metabolized in vivo; approximately 30–90% may be excreted as active compounds via animal urine and feces, and subsequently enter into the environment [6,7].

The excreted antibiotics in manure and other animal waste may be introduced into the agricultural soil through different pathways, including land application, direct excretion

(grazing animals or free-ranging chicken in integrated farming systems) and wastewater [4,8]. After reaching the soil, these antibiotics may be leached or transported to water bodies [9–11]. Antibiotic contamination can cause ecological disturbances and risks to human health [12] via the development and spread of antibiotic-resistant genes in the ecological environment [13–15]. Studies have reported extensive veterinary antibiotics contaminations in agricultural soils, surface water and groundwater systems associated with various hydrological mechanisms, mainly surface runoff and leaching from contaminated sites [16–19].

Among the key processes that remobilize contaminants in agricultural soil, leaching is important for the downward migration of veterinary antibiotics, especially for weakly-sorbing antibiotic species [20,21]. Growing evidence suggests that the extensive presence of manure particles, dissolved organic matter (DOM) and other associated organic colloids may alter the fate and transport potentials of veterinary antibiotics in the environment [22–26]. Vertical migration of veterinary drugs increases the vulnerability of groundwater to pollution danger, and this could be more significant in macroporous soils dominated by preferential flow paths [27,28]. However, leaching studies of veterinary antibiotics on field sites are limited. The few available studies only reported concentration data lacking sufficient information for downgradient risk assessment. Measuring concentration data concurrently with the Darcy velocity of infiltrating water (mass flux) during rainfall events is crucial for regulatory decisions and to circumvent the uncertainty associated with mass flux estimates and laboratory simulations. Nevertheless, studies on antibiotic vertical mass flux in natural field sites under integrated farming systems are still missing.

The potential of manure particles and/or manure-dissolved organic matter (DOM) to mediate the leaching of veterinary antibiotics has been reported in the literature [25,26,29]. DOM can constrain the partitioning, adsorption–desorption and other key processes that influence the leaching potential of veterinary antibiotics through several physical and chemical interaction mechanisms, such as complexation reaction, electrostatic interaction, van der Waals force and hydrophobic partitioning [29–32]. However, a systematic investigation reconciling field and laboratory leaching data are currently unavailable. The potential risk of veterinary antibiotic pollution from manured agricultural farmland requires adequate attention. Therefore, tracking DOM and its optical properties alongside the mass flux of veterinary antibiotics will provide better insights for leaching risk management.

Sulfonamides (sulfadiazine) and chloramphenicol (florfenicol) are important classes of veterinary medicines (Figure S1) mostly consumed in animal husbandry [33,34], and are often reported to interact with DOM in the soil water system as biologically active compounds [31,35,36]. Understanding the mass flux of these antibiotics and the coupling effects of natural field environments in association with manure-DOM under rainfall conditions is essential to prevent antibiotic pollution risks and its potential health hazards. The objectives of this study were to: (1) measure the vertical mass flux of florfenicol (FFC) and sulfadiazine (SDZ) during natural rainfall events in an orchard field site integrated with free-ranging chickens; (2) explore the relationship between the mass flux of the target antibiotics, DOM optical indices and leachate-suspended particles; and (3) compare the leaching mechanism of antibiotics in association with manure-DOM under matrix flow and field conditions.

## 2. Materials and Methods

### 2.1. Chemicals and Reagents

Sulfadiazine (SDZ, C<sub>10</sub>H<sub>10</sub>N<sub>4</sub>O<sub>2</sub>S, CAS-Nr. 68-35-9) and florfenicol (FFC, C<sub>12</sub>H<sub>14</sub>Cl<sub>2</sub>FNO<sub>4</sub>S, CAS-Nr. 73231-34-2) with >99% purity were purchased from Dr. Ehrenstorfer, GmbH (Augsburg, Germany). Stock solutions (1 g L<sup>-1</sup>) of both antibiotics were prepared in HPLC grade MeOH (Merck, Belgium) and finally diluted to 20 L for orchard plot spiking using tap water to obtain a final concentration of 0.05 mg mL<sup>-1</sup>. High-purity reagents for liquid chromatography–mass spectrometry (UPLC-MS/MS) analysis were purchased

from Sinopharm Chemical Reagent Co., Ltd. (Shanghai, China). Isotope-labelled internal standards were used to compensate for antibiotic loss during preparation and matrix effect, and were purchased from Toronto Research Chemicals (Berlin, Germany). Oasis hydrophilic–lipophilic balance (HLB) cartridges (6 mL 200 mg) were purchased from Waters (Milford, MA, USA). Glass fibre filters (pore size, 0.22  $\mu\text{m}$ ) were purchased from Whatman (Maidstone, UK).

## 2.2. Study Site and Experimental Setup

The study was conducted in a small agricultural catchment in the hilly area of central Sichuan, southwestern China. The orchard plots are located at: A ( $105^{\circ} 27' 30''$  E,  $31^{\circ} 16' 8''$  N), B ( $105^{\circ} 27' 30''$  E,  $31^{\circ} 16' 9''$  N) and C ( $105^{\circ} 27' 30''$  E,  $31^{\circ} 16' 9''$  N), at 420 m above sea level (Figure 1). Crop farmlands account for approximately 55% of the area. The region falls under a moderate subtropical monsoon climate with an annual average temperature and rainfall of 17.3  $^{\circ}\text{C}$  and 826 mm, respectively (1981–2006). The soil characteristics, rainfall and hydrological description of the region have previously been documented [37–39].

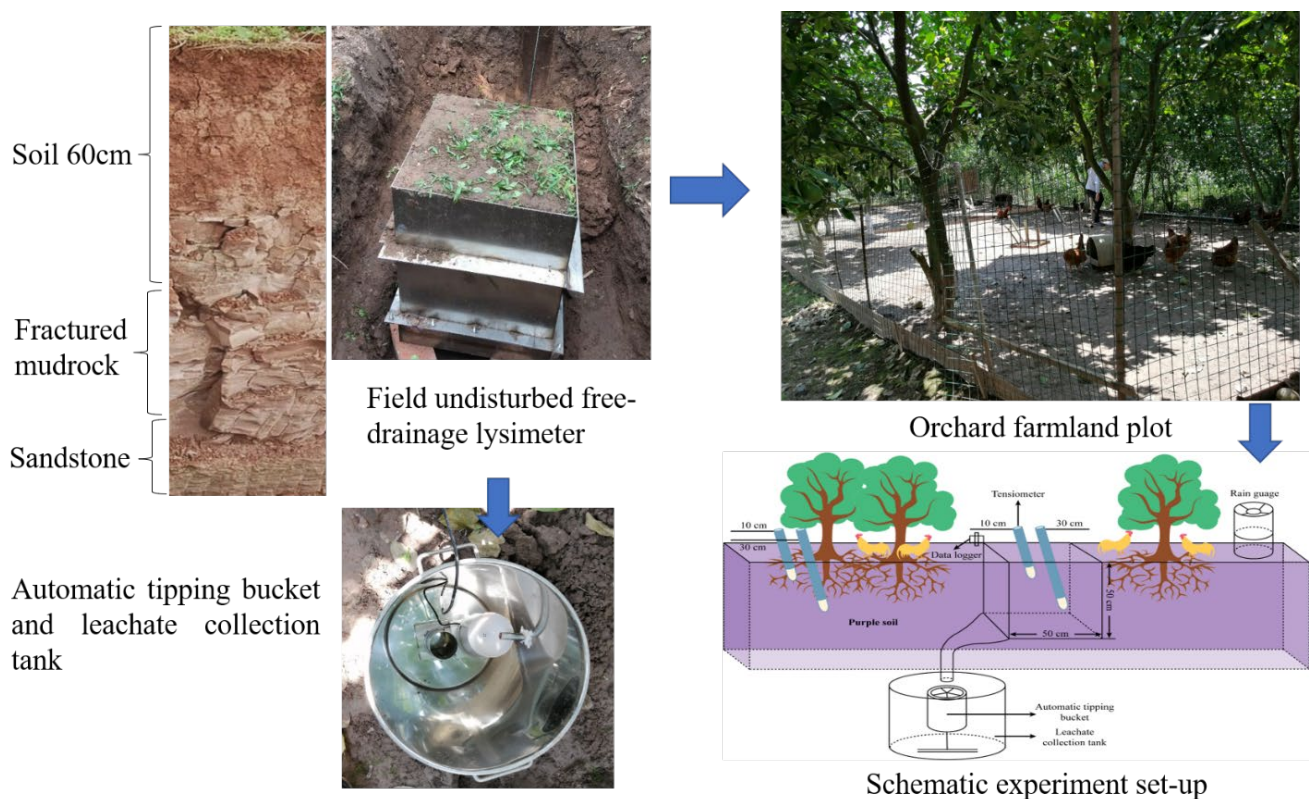


**Figure 1.** Experimental setup of the chicken-integrated orchard farmland, showing the undisturbed field lysimeter installation and tipping bucket placed inside the leachate collecting tank. The schematic diagram gives an overview of the orchard farmland experimental setup.

Three experimental plots named A, B and C ( $122.08 \text{ m}^2$  surface area each) were demarcated with wire gauze in orchard farmland integrated with free-ranging chickens, a well-known traditional agricultural land use in the hilly area of central Sichuan, southwestern China. Plot A was the control (without roaming chickens), while plots B and C were open areas for the free-ranging chickens, but the chicken house was located in plot B. Undisturbed field soil lysimeters ( $50 \text{ cm}$  width,  $50 \text{ cm}$  length,  $50 \text{ cm}$  depth and surface area  $0.25 \text{ m}^2$ ) were technically excavated and reinstalled at the centre of each plot 4 years before the study. The lysimeter bottom boundary was underlain with quartz sand to prevent soil from sliding and blocking the leachate collection furrow. The leachate was

channeled with an aluminum pipe into a tipping bucket rain gauge to quantify the leachate amount. Tensiometers (T4e, UMS, München, Germany) were installed at 10 cm and 30 cm depths inside and outside the lysimeters in plots to monitor the water potential during rainfall events.

In order to control interferences of residual antibiotics in the orchard farmland experiment, our target antibiotics were excluded from the medications administered to the free-ranging chickens in the farming seasons preceding the study. Following that, 0.05 mg mL<sup>-1</sup> FFC and SDZ solution were evenly spiked over the experimental plots (A, B and C), and the lysimeter leachates were collected under four heavy rainfall events in the summer of 2020 (Table 1).

**Table 1.** Rainfall and leachate properties.

| Rainfall Events | Rainfall Amount | Duration | Maximum Intensity | Preceded Dry Days | Average Leachate Discharge per 15 min (cm <sup>3</sup> h <sup>-1</sup> ) |        |        |
|-----------------|-----------------|----------|-------------------|-------------------|--|--------|--------|
|                 | (mm)            | (h)      | (mm/15 min)       | (days)            | Plot A   | Plot B | Plot C |
| 12 August 2020  | 17.2            | 4        | 32.8              | 3                 | 68.13  | 165.31 | 4.06   |
| 13 August 2020  | 46.6            | 17       | 28.8              | 1                 | 104.06   | 89.14  | 28.75  |
| 15 August 2020  | 16              | 5        | 22.4              | 2                 | 145.50   | 226    | 35     |
| 18 August 2020  | 20.2            | 11       | 12                | 3                 | 77.73  | 190.91 | 51.59  |

Plot A was the control (without manure), while plots B and C represented manured plots (chicken-raising orchard plots).

### 2.3. Sampling and Data Collection

#### 2.3.1. Rainfall Events and Field Lysimeter Leachate

A total of four rainfall events (on the 12th, 13th, 15th and 18th August 2020) that generated subsurface flow were monitored in this study. The lysimeter leachate was continuously measured with a tipping bucket connected to a HOBO event data logger (Onset Computer Corp., Bourne, MA, USA), and the soil water potential was recorded with tensiometers (T4e, UMS, München, Germany). The rainfall amount and duration were also recorded using a tipping bucket rain gauge. All data were recorded at 15 min intervals, and after each rainfall event, the lysimeter leachate was thoroughly mixed before being sampled (Table 1).

The first three events were characteristic of heavy rainfall events commonly experienced in the region, while the fourth rainfall event was classified as medium. The lysimeter discharge responded well to each rainfall event, but the leaching rate varied among the plots. The heavy event on 12th August occurred for a shorter duration but at a higher intensity after three preceding dry days, which resulted in less percolation and generated low subsurface flow, especially in plots A and C with discharges of 68.13 cm<sup>3</sup> h<sup>-1</sup> and 4.06 cm<sup>3</sup> h<sup>-1</sup>, respectively. This was associated with longer dry periods that caused changes in the surface soil structure, especially in light-textured purple soil, which altered the rainfall infiltration and increased runoff generation. The subsequent events on 13th and 15th August generated higher discharges of 28.75–104.06 and 35–145.50 cm<sup>3</sup> h<sup>-1</sup>, respectively (Table 1).

#### 2.3.2. Chicken Manure-DOM Extraction and Column Experiments

Manure-DOM was extracted from chicken manure (Table 2) by shaking method. Fresh chicken manure samples were air-dried, sieved with a 60-mesh sieve and extracted with 0.01 mol L<sup>-1</sup> CaCl<sub>2</sub> and 0.1 g L<sup>-1</sup> NaN<sub>3</sub> solution in a 50 mL plastic centrifuge tube. The mixture was shaken at 180 r min<sup>-1</sup> at 25 °C for 16 h, sonicated for 30 min, centrifuged at 25 °C, 8000 r min<sup>-1</sup> for 10 min and finally filtered using 0.45 µm PTFE filter membrane to obtain water-extractable manure-DOM [22,31,33–35].

**Table 2.** Selected properties of the orchard soil and chicken manure.

| Samples        | Sand | Texture |      | pH<br>(-)   | OC<br>(g kg <sup>-1</sup> ) | DOC<br>(mg L <sup>-1</sup> ) | CEC<br>(cmol kg <sup>-1</sup> ) | $\rho$<br>(g cm <sup>-3</sup> ) |
|----------------|------|---------|------|-------------|-----------------------------|------------------------------|---------------------------------|---------------------------------|
|                |      | Silt    | Clay |             |                             |                              |                                 |                                 |
| Orchard soil   | 30%  | 66%     | 4%   | 7.98 ± 0.14 | 15.52 ± 1.11                | 38.2 ± 0.54                  | 18.2 ± 0.64                     | 1.49 ± 0.10                     |
| Chicken manure | ND   | ND      | ND   | 7.28 ± 0.20 | 486.25 ± 2.56               | 7977 ± 3.24                  | 53.41 ± 0.84                    | ND                              |

OC: organic carbon; DOC: dissolved organic carbon; CEC: cation exchange capacity;  $\rho$ : bulk density; ND: not determined.

The effects of chicken manure-DOM on SDZ and FFC leaching behaviour in purple soil were further examined in repacked soil columns under saturated conditions. Composite soil samples were collected from the experimental plots (Table 2), air-dried, sieved (2 mm) and treated with chicken manure-DOM in two ways: (i) pre-coated soil (pre-equilibrated with 100 mg OC/L DOM for 4 days) and (ii) co-transport only (Figure S2) [40].

Columns (15 cm in length, and 1.25 cm inner diameter) were packed at 1 cm increments by gradual tapping with a pestle to ensure uniform packing. Our pre-experiment confirmed that SDZ and FFC sorption onto the column wall was negligible. The bulk density and porosity of the soil columns ranged from 1.43–1.49 g cm<sup>-3</sup> and 0.44–0.46, respectively. All columns were slowly saturated from the bottom with 0.1 g L<sup>-1</sup> NaN<sub>3</sub> and 0.01 mol L<sup>-1</sup> CaCl<sub>2</sub> solution at a steady flow rate of 20.3  $\mu$ L min<sup>-1</sup> for approximately 48 h to keep the ionic strength of the soil solution constant and the soil saturated. Following that, 5 pore volumes (PV) of antibiotics solution (FFC and SDZ) in a combination of manure-DOM and nonreactive tracer (1 mg L<sup>-1</sup> VAs + 100 mg L<sup>-1</sup> DOM + 100 mg L<sup>-1</sup> Br<sup>-</sup>) were injected at a steady flow rate of 162.5  $\mu$ L min<sup>-1</sup> (equivalent to 21.7 mm h<sup>-1</sup> rainfall) and finally eluted with 4 pore volumes (PV) of background solution (0.1 g L<sup>-1</sup> NaN<sub>3</sub> and 0.01 mol L<sup>-1</sup> CaCl<sub>2</sub>).

## 2.4. Analyses

### 2.4.1. Sample Analysis

The concentrations of the target antibiotics (SDZ and FFC) in lysimeter leachate were analyzed using high-performance liquid chromatography–tandem mass spectrometry (Framingham, MA, USA). The analytical column consisted of a BEH C18 column (2.1 × 100 mm, 1.7  $\mu$ m, Waters, Milford, MA, USA). Lysimeter leachate (2 L) was acidified, filtered through a 0.45  $\mu$ m PES membrane (Millipore, Billerica, MA, USA) and isotopic standards were added before being loaded into a pre-conditioned Oasis HLB cartridge. The analytical conditions of the HPLC-MS and the solid phase extraction procedure were adapted as described in previous studies [21,35,41,42].

Some selected parameters, including pH, EC, DOC, colloid concentration and particle size distribution (PSD), were measured within 24 h after sampling. The pH was measured with pH meter (Leici Environmental Co, Shanghai, China), and colloid concentration was determined after 2 min of ultrasound (100 W) in water bath sonicate (KQ-3000VDE, Huqin Equipment Co., Ltd., Shanghai, China) by spectrophotometer (Tu-1810, Purkinje General Instrument Co., Beijing, China). The distribution of particles in lysimeter leachate was measured by laser scattering particle size distribution analyzer (LA950, Horiba, Kyoto, Japan), and DOC was measured by TOC analyzer (OI Analytical Aurora 1030C, TX, USA).

Furthermore, the UV-visible absorbance (200 to 600 nm) and excitation–emission matrix (EEM) fluorescence (at emission wavelengths from 250–800 nm, and excitation wavelength from 240 to 600 nm) of the leachate samples were obtained via Aqualog fluorescence spectrometer (Horiba JY Aqualog, Japan) at 1 nm increments and an integration time of 0.5 s. The results were corrected for inner-filter effects, Raman bands and Rayleigh scatters, and instrument-specific spectral biases were removed. The spectral peaks were investigated using parallel factor (PARAFAC) analysis [43] and optical indices were calculated to describe the compositional characteristics of the leachate DOM: (1) SUVA<sub>254</sub> describes the aromaticity of DOM and it is the ratio of UV absorbance at 254 nm (m<sup>-1</sup>) and DOC concentration (mg-C L<sup>-1</sup>); (2) humification index (HIX) was calculated as the ratio of the peak integrated area from 435 to 480 nm and the sum of the emission spectra over

300–345 nm and 435–480 nm at an excitation of 254 nm; (3) spectral slope ratio (SR) was calculated by dividing  $S_{275-295}$  by  $S_{350-400}$  [41–43].

#### 2.4.2. Mass Flux of SDZ and FFC

Mathematically, the mass flux ( $J$ ) of the target antibiotics passing through the cross-sectional area of the undisturbed field lysimeter ( $50 \times 50 \times 50$  cm) in orchard–chicken-integrated farmland during rainfall can be calculated as follows:

$$J = qC \quad (1)$$

$$q = -K \frac{\partial h}{\partial z} \quad (2)$$

where  $J$  is the mass flux ( $\text{ML}^{-2} \text{T}^{-1}$ ),  $q$  is Darcy flux ( $\text{LT}^{-1}$ ) calculated using the tipping bucket leachate flow data recorded at 15 min intervals,  $C$  is the antibiotic concentration in the liquid phase ( $\text{ML}^{-3}$ ),  $K$  is hydraulic conductivity ( $\text{LT}^{-1}$ ),  $\partial h/\partial z$  is the hydraulic gradient (dimensionless).

### 2.5. Modelling

#### 2.5.1. One-Dimensional Transport and Sorption Parameters

A convection–dispersion equation for one-dimensional transport behaviour of the target antibiotics in repacked soil columns fitted with HYDRUS-1D [44] is based on two concepts: (1) two kinetic retention sites and (2) two-site chemical nonequilibrium adsorption model [44–47] with Freundlich adsorption isotherm implemented.

#### 2.5.2. Two-Site Nonequilibrium Adsorption Model

This model conceptually divides the sorption sites into two fractions. It assumes that adsorption on Type 1 sites is instantaneous, while adsorption on the other fraction (Type 2 sites) is kinetically controlled [46–48]:

$$S = S^e + S^k \quad (3)$$

where  $S^e$  and  $S^k$  ( $\text{M M}^{-1}$ ) are fractions of the sorption sites assumed to be instantaneous and kinetically controlled on Type 1 and Type 2 (first-order kinetic rate), respectively.

Thus, the conventional advection–dispersion equation is modified as follows:

$$\frac{\partial \theta c}{\partial t} + \rho \frac{\partial S^e}{\partial t} + \rho \frac{\partial S^k}{\partial t} = \frac{\partial}{\partial z} \left( \theta D \frac{\partial c}{\partial z} \right) - \frac{\partial qc}{\partial z} - \phi \quad (4)$$

$$S^e = f_e K_f C^\eta \quad (5)$$

$$\rho \frac{\partial S^k}{\partial t} = \alpha_k \rho (S_e^k - S^k) - \phi_k \quad (6)$$

$$S_e^k = \alpha_k (1 - f_e) K_f C^\eta \quad (7)$$

The bromide BTC was fitted to obtain dispersivity  $\lambda$  (cm):

$$\lambda = D/v \quad (8)$$

where  $\rho$  is the porosity ( $\text{L}^3 \text{L}^{-3}$ );  $t$  is time (T);  $c$  is the solution concentration ( $\text{M L}^{-3}$ );  $S^e$  and  $S^k$  are the sorbed concentrations on equilibrium and kinetic sorption sites ( $\text{M M}^{-1}$ ), respectively;  $\theta$  is the water content ( $\text{L}^3 \text{L}^{-3}$ );  $D$  is the hydrodynamic dispersion coefficient ( $\text{L}^{-2} \text{T}^{-1}$ );  $\lambda$  is dispersivity,  $v$  is pore velocity,  $z$  is the depth (L);  $\rho$  is the bulk density ( $\text{M L}^{-3}$ );  $f_e$  is the fraction of sorption sites in equilibrium with liquid phase (dimensionless);  $K_f$  is the Freundlich distribution coefficient ( $\text{M}^{1-\eta} \text{L}^{3\eta} \text{M}^{-1}$ );  $\eta$  is the dimensionless Freundlich

exponent;  $\alpha_k$  is the first-order rate coefficient associated with the kinetic site ( $T^{-1}$ );  $\phi$  is the sink term ( $n L^{-3} T^{-1}$ );  $v$  is the average pore water velocity ( $cm\ min^{-1}$ ).

### 2.5.3. Two Kinetic Site Model

The two kinetic site model (Equations (9)–(11)) assumes that adsorption kinetically occurs on both fractions of the sorption sites and proceeds at different rates, which can be written as:

$$\frac{\partial \theta c}{\partial t} + \rho \frac{\partial S_1^k}{\partial t} + \rho \frac{\partial S_2^k}{\partial t} = \frac{\partial}{\partial z} \left( \theta D \frac{\partial c}{\partial z} \right) - \frac{\partial q c}{\partial z} - \phi \quad (9)$$

$$\rho \frac{\partial S_1^k}{\partial t} = k_{a1} \theta c - k_{d1} \rho S_1^k - \phi_{k1} \quad (10)$$

$$\rho \frac{\partial S_2^k}{\partial t} = k_{a2} \theta c - k_{d2} \rho S_2^k - \phi_{k2} \quad (11)$$

where  $\partial S_1^k$  and  $\partial S_2^k$  are the sorbed concentrations of the first and second kinetic sorption sites ( $M\ M^{-1}$ ), respectively;  $k_{a1}$  and  $k_{a2}$  are the attachment coefficients of the first and second fraction of kinetic sorption sites ( $T^{-1}$ ), respectively;  $k_{d1}$  and  $k_{d2}$  are the detachment coefficients of the first and second fraction of kinetic sorption sites ( $T^{-1}$ ), respectively;  $\phi_{k1}$  and  $\phi_{k2}$  are the sink terms for the first and second kinetic sorption that represent various reactions at the kinetic sorption sites ( $n L^{-3} T^{-1}$ ).

### 2.5.4. Data Analysis

The mass flux of the target antibiotics in field lysimeter leachate was calculated (Equations (1) and (2)) and one-way ANOVA statistical analyses were conducted using SAS version 9.4 (SAS Institute, Cary NC, USA) to compare the mass flux of the two antibiotics (SDZ and FFC). Significant differences were considered at  $p < 0.05$ . DOM optical properties were investigated using fluorescence excitation–emission matrix coupled with parallel factor analysis (EEM-PARAFAC). Redundancy analysis was performed using CANOCO version 5.0 (Microcomputer Power, Ithaca, NY, USA) to evaluate the relationship between EEM-PARAFAC components, DOM and its optical indexes, suspended particles and antibiotics mass flux.

## 3. Results and Discussion

### 3.1. Soil Water Flow Dynamics Corresponding to Natural Rainfall Events

Soil water potential is usually used to infer water movement in soil, and it is a valuable tool for understanding antibiotic mass flux in macroporous soil. The water potential of the three experimental plots (A, B and C) continuously monitored during the four rainfall events (Table 1) showed that the lysimeter soil profiles were saturated during the rainfall events (Figure 2), as recorded at 10 cm and 30 cm profile depths (water potential  $> 0$  cm). The water potential indicated consistent soil water penetration into the lysimeter soil profile depth during the first rainfall event (12 August 2020) with the highest maximum intensity ( $32.8\ mm\ h^{-1}$ ) but a short duration (4 h). The trend in control plot A showed earlier and higher saturation at the lower soil depth (30 cm) than at the upper soil depth (10 cm depth). Interestingly, the two observation depths (10 cm and 30 cm) indicated a similar soil water response to the rainfall event. Additionally, similar trends in soil water potentials were observed at 10 cm and 30 cm profile depths of plots B and C, which were almost overlapping.

The second rainfall event came after 24 h with a lower maximum intensity ( $28.8\ mm/h$ ) but with a longer duration (17 h). During the rainfall event, the soil profile wetting followed a similar pattern as was observed during rainfall event 1. It is worth noting the consistently higher water saturation level at the lower soil depth (30 cm depth) than at the upper depth (10 cm depth) in control plot A under each of the four rainfall events monitored (Figure 2). A similar scenario was observed in manured plot B during events 1 and 3, as well as in manured plot C during events 3 and 4 (Figure 2). Earlier and higher saturation levels of

the lower soil depth suggest that the infiltrating water may have bypassed the upper soil profile to saturate the lower depth through preferential flow channels. A similar result was also observed for the water potential measured in the open field within the experimental plot (Figure S3). This result confirmed the abundance of rapid subsurface flow channels such as root holes, wormholes, interaggregate pore spaces and preferential flow channels peculiar to macroporous soils. This phenomenon has been reported in previous studies conducted at different locations on the same study site [37–39]. Subsurface flow is the main pathway for contaminant transport in the region, accounting for over 88% of runoff. According to Wang (2013), the saturated hydraulic conductivity ( $K_s$ ) of the region ranged from 37 to 43  $\text{mm h}^{-1}$  (for 10–15 cm depth), while Zhang et al. (2016) reported 17.6  $\text{mm h}^{-1}$  (for 25–30 cm depth) and 12.9  $\text{mm h}^{-1}$  for the fractured mudrock region [37,38,49]. As such, the hydrological condition of the region influences the water quality status of the Yangtze River.

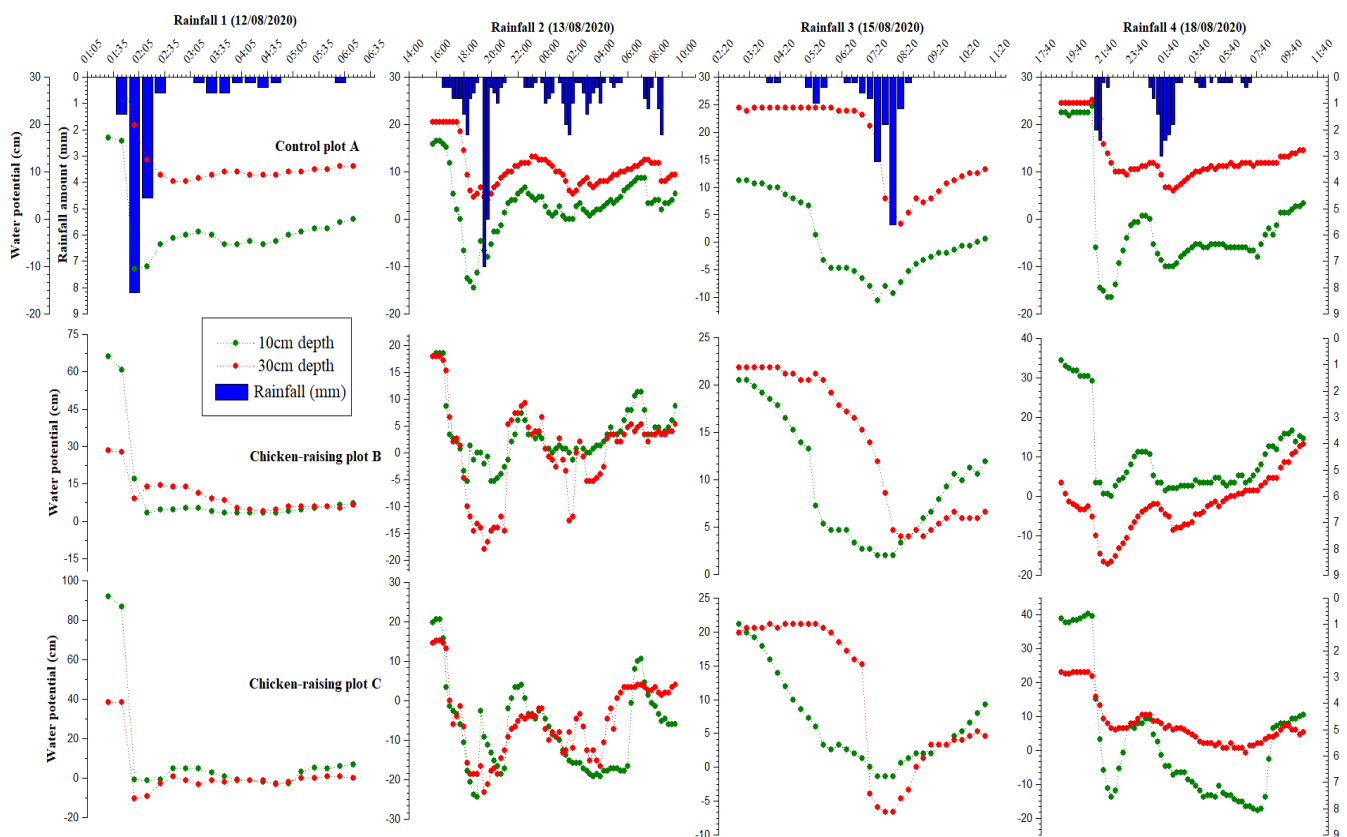


**Figure 2.** Temporal and spatial variability of water potential at 10 cm and 30 cm depth continuously measured inside the field lysimeter during the four rainfall events (1–4) observed. Control plot A is a plot without chicken manure, plots B and C are manured plots (with free-ranging chickens). Red line with red symbols represents water potential trend at 10 cm depth, while green line with green symbols depicts water potential trend at 30 cm depth.

### 3.2. Mass Flux of Sulfadiazine and Florfenicol in Lysimeter Leachate

The mean overall mass fluxes of SDZ and FFC in lysimeter leachate under the four rainfall events observed are shown in Figure 3. SDZ showed significantly higher leaching and migration potential (ranging from 2.7 to 6.6  $\mu\text{g m}^{-2} \text{h}^{-1}$ ) compared to FFC across the three plots (A, B and C). The mass flux of SDZ in manured plots B and C (4.2 and 2.7  $\mu\text{g m}^{-2} \text{h}^{-1}$ , respectively) was considerably lower compared to 6.6  $\mu\text{g m}^{-2} \text{h}^{-1}$  in control plot A. High leaching potential of SDZ to groundwater has been reported in the literature [38,39]. It was also suggested that the presence of manure and/or manure-DOM

may increase SDZ adsorption tendency in the soil [49–53], but the retention potential in the soil profile depends on the soil hydrological processes and rainfall properties.

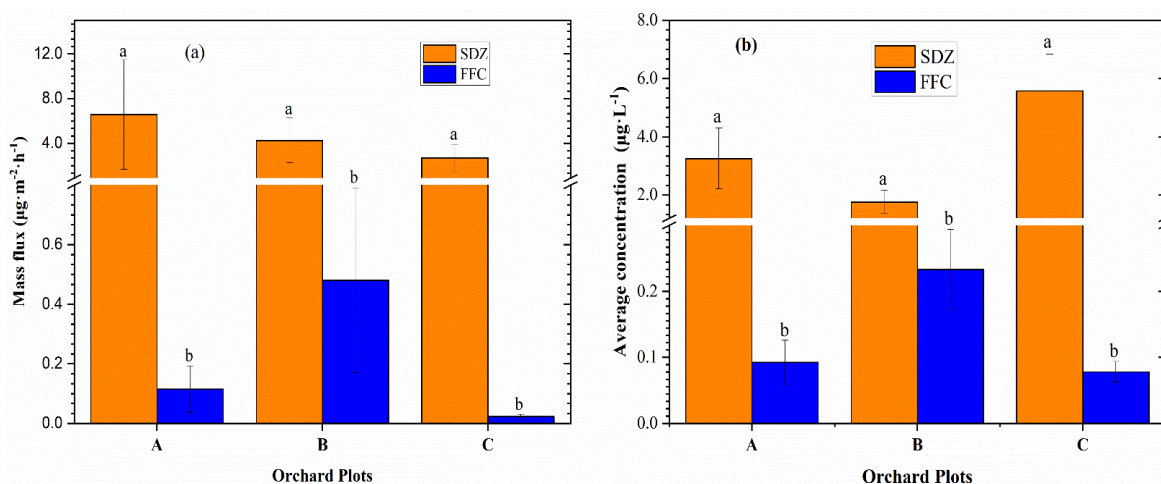


**Figure 3.** Mean comparison of mass flux (a) and average leaching concentration (b) of sulfadiazine (SDZ) and florfenicol (FFC) in orchard plots' lysimeter leachate under natural rainfall events. Lowercase letters a and b indicate statistical differences between the antibiotic mass flux (ANOVA  $p < 0.05$ ). Capital letter A represents the control plot (without manure), while B and C are manured orchard plots.

Contrastingly, the mass flux of FFC was generally low across the orchard field plots (Figure 3). The lowest mass fluxes of  $0.12$  and  $0.02 \mu\text{g m}^{-2} \text{h}^{-1}$  were observed in control plot A and manured plot C (which is rarely visited by the ranging chickens), respectively. The mass flux in manured plot B was moderately higher ( $0.48 \mu\text{g m}^{-2} \text{h}^{-1}$ ), suggesting facilitated transport of FFC in manured plots. The observed FFC transport behaviour in an undisturbed field lysimeter contradicts the findings of Tang et al., (2021) using column studies, where FFC mobility was reportedly reduced in manure-amended soils [54].

The antibiotic mass flux was further examined based on each rainfall event monitored (Figure 4). Statistical analysis confirmed significantly higher FFC mass flux in manured plot B compared to other plots, especially under events 1, 3 and 4. The first rainfall event with the highest maximum intensity ( $32.8 \text{ mm/h}$ ) but a short duration (4 h) generated the highest mass flux. However, the reduced mass flux of FFC under events 2, 3 and 4 suggested a possible interaction of FFC with chicken manure and/or mobile manure-DOM. On the other hand, SDZ mass fluxes in control plot A during rainfall events 1, 2 and 4 were significantly lower, except under rainfall event 3. Similarly, the mass fluxes of SDZ in plots B and C (with chicken manure) were reasonably higher than in plot A (control), except during event 3. Overall, SDZ showed strong leaching potential in control plot A (no manure), while FFC was more prone to leaching in manured orchard purple soil.

### 3.3. EEM-PARAFAC Components during Rainfall Events

The EEM-PARAFAC analysis of the lysimeter leachate under rainfall events monitored showed that the DOM contained three main PARAFAC components. These were designated as Component 1 (C1) at excitation/emission (Ex/Em) wavelengths of  $270(380)/430 \text{ nm}$ , Component 2 (C2)  $260(400)/480 \text{ nm}$  and Component 3 (C3)  $270/370 \text{ nm}$  (Figure 5 and Table S1). Previous studies have classified components C1 and C2 as typical UVA humic-like components consisting of fulvic-acid-like materials, while component C3 is a characteristic protein-like substance [55–57]. The distribution and the relative abundance of DOM and the EEM-PARAFAC components C1, C2 and C3 are shown in Figure 6. The proportions of DOC (with ranges from 42 to 54%) and components C1 (with ranges from 44 to 47%) in the control plot were consistently higher than in the manured plots (B and C) during the rainfall events (1, 2 and 3). Interestingly, control plot A had the lowest proportions of

components C2 and C3, while manured plots B and C showed considerably higher proportions of components C2 and C3, with C2 ranging from 16 to 51% and 28 to 73% for plots B and C, respectively. Similarly, C3 ranged from 23 to 53% and 15 to 61% for plots B and C, respectively. Thus, the disproportionate contents of DOM and PARAFAC components measured in the leachate samples may have had important implications for the differences observed in SDZ and FFC mass fluxes across the studied plots. For example, the higher mass fluxes of SDZ and FFC in plot B coincided with the higher proportions of components C2 and C3 observed in its leachate samples. Similarly, a higher proportion of DOC and component C1 observed in the leachate samples from control plot A may be related to the significantly higher mass flux of FFC under rainfall event II. Likewise, the high proportions of components C2 and C3 in plots A and B might be linked to the significantly higher mass fluxes of SDZ in their leachate (Figures 5 and 6). These findings suggest that PARAFAC components influenced the mass fluxes of FFC and SDZ in our experimental plots, and that the specific impact may have varied depending on the distribution of the components and their interaction with antibiotic species.

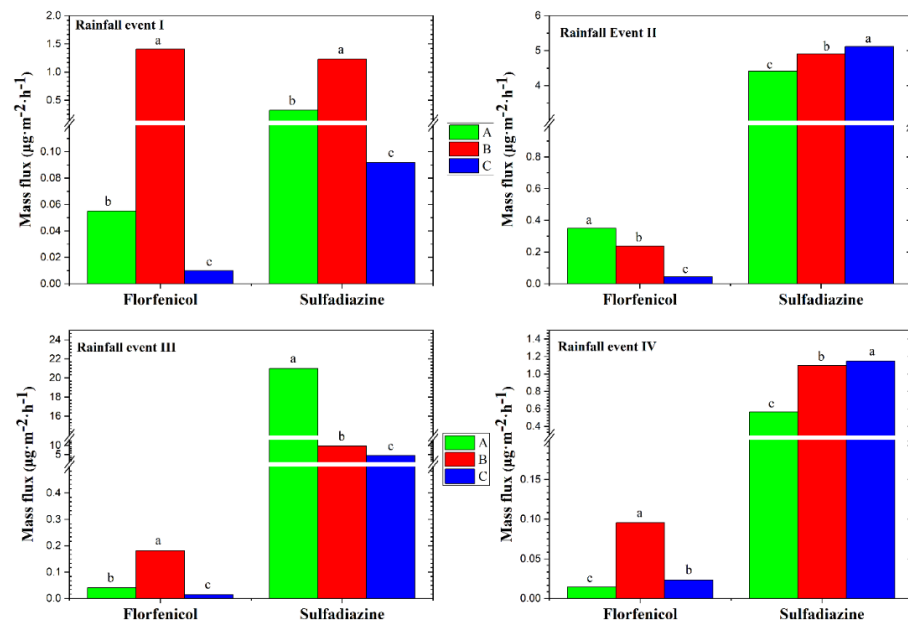


**Figure 4.** Mass flux of florfenicol (FFC) and sulfadiazine (SDZ) in orchard farmland under natural rainfall events (rainfall events I–IV). Lowercase letters indicate statistical differences between the antibiotic mass flux (ANOVA  $p < 0.05$ ). A represents the control plot (without manure), B and C are manured plots.

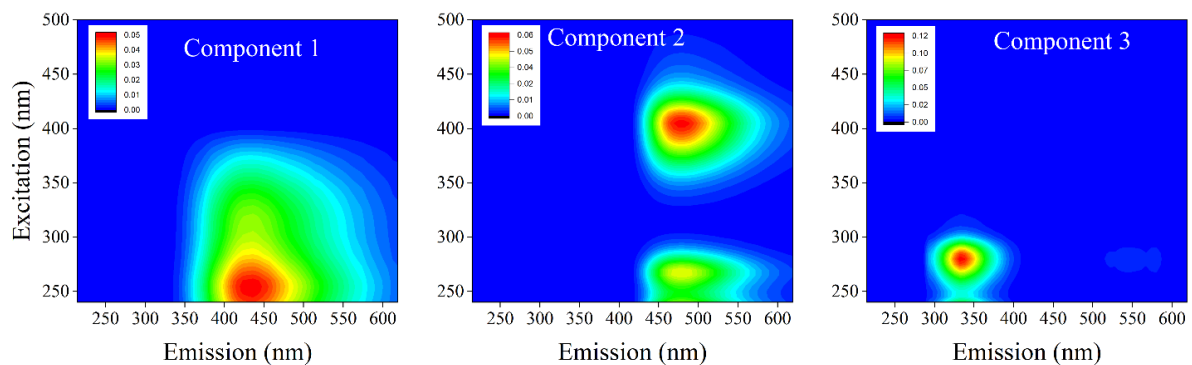


**Figure 5.** Excitation–emission matrix spectra of three DOM PARAFAC components found in orchard plot leachate. **Component 1** (C1) is a short-wave humus; **Component 2** (C2) is a long-wave humus consisting of a humic-like component and a tyrosine-like component; and **Component 3** (C3) is a tryptophan-like component.

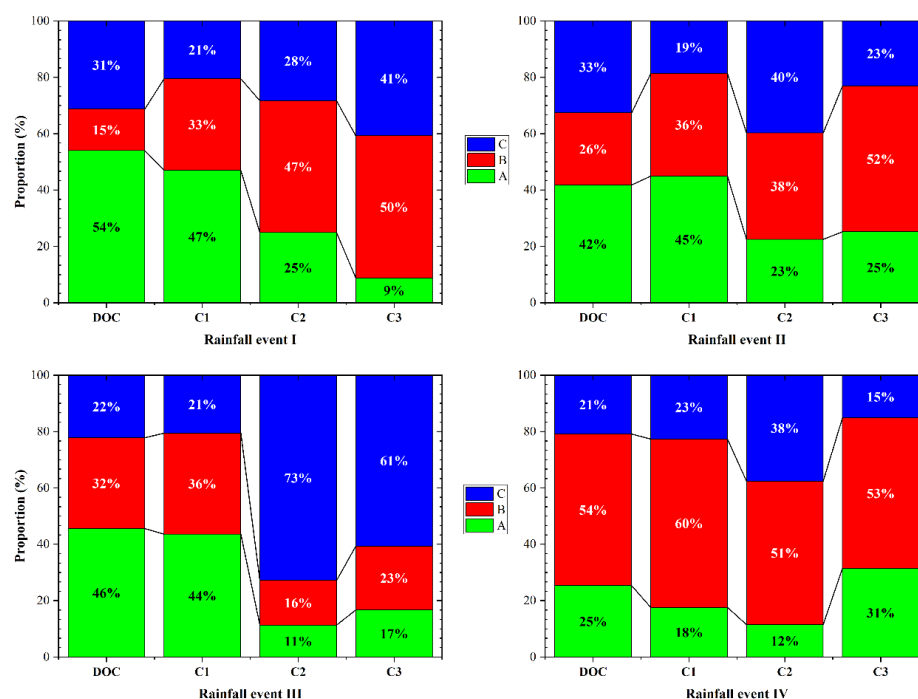


**Figure 6.** Distribution of DOC and EEM-PARAFAC components under natural rainfall events (rainfall events I–IV). (A) represents the control plot (without manure), (B) and (C) are the manured plots (with free-ranging chickens).

### 3.4. Response of Antibiotics Mass Flux to DOC and Optical Indices of DOM

Redundancy analysis (RDA) was conducted to better understand the specific relationship between the antibiotic (FFC and SDZ) mass flux and DOM optical indices (Figure 7 and Table S1). The result showed that the combined effects of DOM optical indices and suspended microparticles ( $PSD < 10 \mu m$ ) accounted for 93.9% of the total variation in SDZ and FFC mass flux observed in the orchard plots. The influencing variables C1, DOC,  $PSD < 10 \mu m$  and HIX accounted for 27.9%, 23.1%, 12.8% and 12.7% of the total variation, respectively. FFC had a close positive relationship with C1,  $PSD < 10 \mu m$ , and a negative relationship with  $S_R$ , while SDZ was more related to C2,  $SUVA_{254}$  and HIX. RDA suggests that DOC and colloids may have negative impacts on SDZ mass flux. The results indicated a strong association between the environmental variables and the mass flux of antibiotics in orchard purple soil. It can be inferred that DOM with a high proportion of PARAFAC components C1 and C3 will enhance FFC leaching in the farmland soil, and this could be more significant in flow channels dominated by a high proportion of water-suspended microparticles  $< 10 \mu m$ . These results corroborated previous studies that reported significant correlations between PARAFAC-derived DOM components and various classes of antibiotics, including sulfonamides, tetracycline, quinolones and macrolides, as well as their occurrence and ecological risks using RDA [58,59]. Therefore, the optical indices of DOM may have considerable impacts on antibiotics' leaching behaviour in farmland soil.

### 3.5. FFC and SZD Breakthrough Curves in Repacked Soil Columns

The breakthrough curve (BTC) of nonreactive bromide tracer indicates that the incorporation of DOM does not affect the column soil structure (Figure 8). Similarly, the bromide BTCs adequately conformed to the physical equilibrium model, confirming the absence of preferential flow channels in the transport domain of the repacked columns. However, the fitted dispersity ( $\lambda$ ) obtained from bromide BTC (0.7 and  $\sim 1.2$  for control and DOM-treated columns, respectively) indicated flow heterogeneity related to the packing process. These water flow parameters were used to simulate SDZ and FFC transport to account for possible variations in the flow domain.

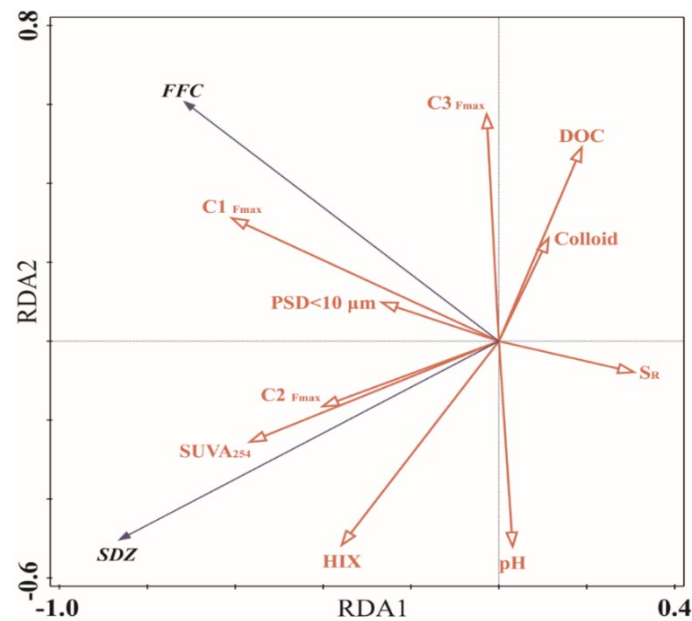


**Figure 7.** Redundancy analysis (RDA) results show the relationships between the target antibiotics (black arrows) and DOM optical indices and soil-released colloids (red arrows). FFC and SDZ represent florfenicol and sulfadiazine, respectively; C1, C2 and C3 are PARAFAC components, HIX: humification index, SR: spectra slope ratio,  $SUVA_{254}$ : specific UV-visible absorbance, PSD < 10  $\mu\text{m}$  sum of particle size distribution < 10  $\mu\text{m}$ .

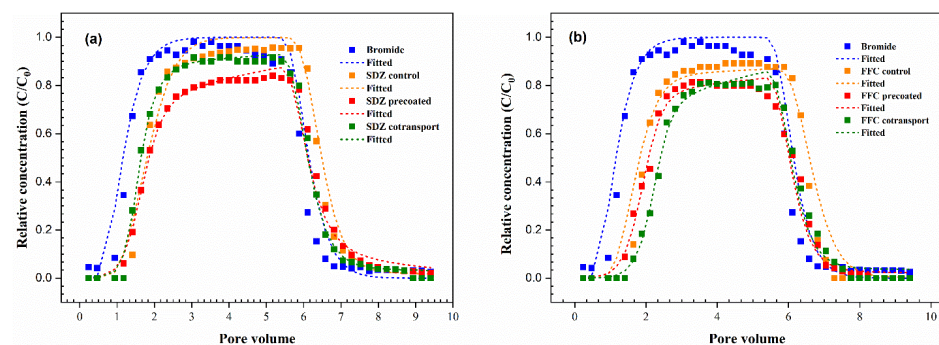


**Figure 8.** Breakthrough curves of sulfadiazine (SDZ) (a) and florfenicol (FFC) (b) from saturated orchard soil column under DOM influence fitted to two kinetics sorption site model. Measured (symbols) versus simulated (lines).

The BTC of SDZ and FFC in the presence and absence of manure-DOM treatments were reasonably delayed relative to nonreactive bromide tracer (Figure 8). Bromide BTC occurred after 0.2 PV compared to SDZ, of which the peak appeared at approximately 1.4, 1.2 and 1.4 PV in control and manure-DOM-treated columns (pre-coated and cotransport conditions), respectively. SDZ BTCs were relatively delayed in the control and DOM co-transport conditions compared to the DOM pre-coated condition. Similarly, FFC BTC in the control and the DOM co-transport column were 1.6 PV delayed, while the DOM pre-coated condition led to a 1.4 PV delay. Overall, the FFC BTC showed a higher relative delay than SDZ under manure-DOM treatment conditions.

Additionally, the antibiotics showed lower BTC peak maxima compared to bromide tracer. The maximum relative concentrations ( $C/C_0$ ) of Br, SDZ and FFC BTC were in the order of Br (0.98) > SDZ (0.96) > FFC (0.89), Br (0.98) > SDZ (0.84) > FFC (0.81) and Br (0.98) > SDZ (0.92) > FFC (0.81) for control, DOM pre-coated and DOM co-transport treatment conditions, respectively. The lower peak maxima of SDZ and FFC indicated the reactive transport and sorbing nature of the antibiotics in the presence of manure-DOM.

This result aligned with previous studies that revealed delayed peak maxima of SDZ in the presence of manure, while FFC leaching was enhanced in the presence of manure colloid [26,59].

It is worth noting that a complete breakthrough of SDZ was not achieved in the control and DOM pre-coated columns within the experimental duration (48 h), as shown by the pronounced tailing in Figure 8. However, a complete breakthrough of SDZ under the DOM co-transport treatment condition was achieved after 8.9 PV. It can be inferred that DOM pre-coating may increase SDZ adsorption and retardation in the soil profile. This result substantiates previous studies that reported incomplete breakthroughs of SDZ after three weeks of experimental duration [60]. Contrarily, FFC complete breakthrough was achieved in all DOM treatment conditions and control, but the breakthrough time varied. The complete breakthrough of FFC was achieved after 7.3 PV, 7.8 PV and 8.5 PV under control, DOM pre-coated and co-transport conditions, respectively. This early breakthrough of FFC can be associated to its weakly hydrophobic nature, which promotes weak adsorption and less retardation in soil [26].

### 3.6. Simulated SDZ and FFC Breakthrough Curves

The BTCs of SDZ and FFC were fitted by two different transport models (Equations (3)–(7) and (9)–(11)), as shown in Figure 8 and Figure S4. The fitted parameters, model statistics and the calculated eluted mass (EM) fractions are given in Table 3 and Table S2. The simulated results confirmed that the eluted mass fraction of SDZ (which ranges from 84 to 96%) was considerably higher than FFC (which ranges from 81 to 89%). The presence of DOM substantially reduced SDZ leaching, with the DOM pre-coating technique having the most considerable impact on SDZ transport (EM of 84%), while the DOM co-transport condition slightly lowered the EM fraction to 91.64%. Unold et al. (2009) previously noted that the transport of SDZ in the presence of manure resulted in lower BTC peaks and slightly lower eluted mass compared to control columns without manure. This was associated to extensive sorption of SDZ to immobile manure particles and soil matrix in repacked soil columns. Similarly, Sukul et al., (2008) observed an increased sorption tendency ( $K_d$  ranging from 6.9 to 40.2) for SDZ in the presence of manure under agricultural soils of various physicochemical properties. Similarly, the co-transport of SDZ with manure-DOM was reported to pose minor relevance to the eluted mass deficit of SDZ [61].

**Table 3.** Fitting parameters of two kinetic sorption sites models.

| Antibiotics | Column       | $k_{a1}$ (min <sup>-1</sup> )                          | $k_{a2}$ (min <sup>-1</sup> )                          | $k_{d1}$ (min <sup>-1</sup> )                          | $k_{d2}$ (min <sup>-1</sup> )                          | R <sup>2</sup> | RMSE                  | EM%   |
|-------------|--------------|--|--|--|--|----------------|-----------------------|-------|
| SDZ         | Control      | $4.78 \times 10^{-3}$<br>( $\pm 8.70 \times 10^{-4}$ ) | 0.36<br>( $\pm 0.02$ )                                 | $5.24 \times 10^{-4}$<br>( $\pm 8.9 \times 10^{-5}$ )  | 1.13<br>( $\pm 0.02$ )                                 | 0.988          | $5.31 \times 10^{-2}$ | 95.70 |
| SDZ         | Pre-coated   | 0.025725<br>( $\pm 0.01$ )                             | $1.55 \times 10^{-3}$<br>( $\pm 2.3 \times 10^{-4}$ )  | $4.20 \times 10^{-3}$<br>( $\pm 8.8 \times 10^{-4}$ )  | $1.15 \times 10^{-6}$<br>( $\pm 6.49 \times 10^{-5}$ ) | 0.990          | $1.61 \times 10^{-2}$ | 84.07 |
| SDZ         | Co-transport | 0.033289<br>( $\pm 3.7 \times 10^{-3}$ )               | $6.07 \times 10^{-4}$<br>( $\pm 2.75 \times 10^{-5}$ ) | $1.16 \times 10^{-6}$<br>( $\pm 3.20 \times 10^{-5}$ ) | $6.58 \times 10^{-4}$<br>( $\pm 1.60 \times 10^{-5}$ ) | 0.995          | $1.21 \times 10^{-2}$ | 91.64 |
| FFC         | Control      | $8.35 \times 10^{-4}$<br>( $\pm 3.18 \times 10^{-5}$ ) | 0.16( $\pm 0.06$ )                                     | $3.36 \times 10^{-5}$<br>( $\pm 1.18 \times 10^{-4}$ ) | 0.32491<br>( $\pm 2.9 \times 10^{-3}$ )                | 0.973          | $7.87 \times 10^{-2}$ | 89.21 |
| FFC         | Pre-coated   | 0.03<br>( $\pm 4.00 \times 10^{-3}$ )                  | $1.28 \times 10^{-3}$<br>( $\pm 8.99 \times 10^{-5}$ ) | $3.46 \times 10^{-4}$<br>( $\pm 7.98 \times 10^{-5}$ ) | $1.23 \times 10^{-5}$<br>( $\pm 5.29 \times 10^{-5}$ ) | 0.987          | $1.85 \times 10^{-2}$ | 81.32 |
| FFC         | Co-transport | 0.05<br>( $\pm 4.95 \times 10^{-3}$ )                  | $1.73 \times 10^{-3}$<br>( $\pm 9.83 \times 10^{-5}$ ) | $9.46 \times 10^{-6}$<br>( $\pm 2.61 \times 10^{-5}$ ) | $3.16 \times 10^{-4}$<br>( $\pm 3.02 \times 10^{-5}$ ) | 0.989          | $3.73 \times 10^{-2}$ | 81.13 |

$k_{a1}$  is the first-order retention coefficient on Type 1 site,  $k_{d1}$  is the first-order detachment coefficient on Type 1 site,  $k_{a2}$  is the first-order detachment coefficient on Type 2 site,  $k_{d1}$  is the first-order detachment coefficient on Type 2 site; R<sup>2</sup>: coefficient of determination; RMSE: root mean square error. 95% confidence intervals are given in brackets. SDZ is sulfadiazine, FFC is florfenicol and pre-coated and co-transport conditions are manure-DOM treatment conditions.

It is worth noting that distinct physical differences were not observed for FFC BTCs under all treatment conditions; both the pre-coated and co-transport DOM conditions equally reduced the EM fraction (~81%). Since this study was conducted within a short duration (48 h), we assumed biodegradation was negligible. Therefore, the mass deficit ob-

served suggests multifaceted interactions between antibiotics-DOM-soil systems, including complexation reaction, co-adsorption and hydrophobic partitioning of immobile particles and soil matrix [29,31,32].

The model statistics confirmed that the TSM and TKS models well represented the BTCs of SDZ and FFC (Table 3 and Table S2). The coefficient of determination ( $R^2$ ) ranged from 0.988 to 0.995 and 0.973 to 0.989 for SDZ and FFC, respectively, with low root mean square error (RMSE). The maximum peak concentration of SDZ under the DOM pre-coated treatment was vastly overestimated by the TSM model (Figure S4a), except for the rising and decreasing limbs of the BTC, which were reasonably well fitted. The fitted TSM-Freundlich sorption model parameter of SDZ showed that the fraction of adsorption sites responsible for instantaneous sorption ( $f$ ) decreased in the presence of DOM from 0.30 in the control to 0.09 and 0.13 for the DOM pre-coated and co-transport conditions, respectively. On the other hand, the  $f$  value for FFC increased from 0.06 (control) to 0.10 and 0.22 for the DOM pre-coated and co-transport conditions, respectively. Similarly, Table S2 shows that the fitted Freundlich adsorption constant ( $K_f$ ) reasonably increased in the presence of DOM from 0.63 to 2.93 and 8.29 for SDZ, and from 9.74 to 13.04 and 33.19 for FFC. These results indicate the occurrence of irreversible antibiotic sorption in the repacked soil columns and explain the low elution mass fractions observed.

The fitted TKS model parameters (Table 3) also indicated that the presence of DOM increased the antibiotics' attachment rate to site 1 ( $k_{a1}$ ), and decreased the attachment rate to site 2 ( $k_{a2}$ ), while the corresponding detachment rates on both kinetic sites ( $k_{d1}$  and  $k_{d2}$ ) were reduced. The results further explain the reason for the incomplete elution and increased  $K_f$  values observed in the presence of manure-DOM. Furthermore, the optimized kinetic sorption rate coefficient ( $\alpha$ ) of SDZ and FFC was decreased in the presence of manure-DOM and stayed approximately stable (Table 3). The decrease in the  $\alpha$  value for SDZ and FFC in the presence of manure-DOM implies reduced mobility of the antibiotics in the column.

#### 4. Conclusions

The mass fluxes of SDZ and FFC in orchard farmland with free-ranging chickens were investigated. The leaching displacement experiments of SDZ and FFC were further conducted in repacked laboratory soil columns under chicken manure-DOM treatment conditions. Field monitoring revealed significant leaching of SDZ in manured plots. Further investigations revealed a strong SDZ correlation with C2, SUVA<sub>254</sub> and HIX. Characteristic preferential flow channels previously established in the study site were validated in this study and were believed to have enhanced the high mass flux of SDZ in manured plots. However, the mass flux of FFC was considerably lower compared to SDZ under all treatment conditions. PARAFAC components (C1 and C3) and PSD < 10  $\mu\text{m}$  were found to be closely associated with FFC mass flux.

Contrary to the increased leaching behaviour of SDZ and FFC in field plots, the presence of manure-DOM increased their retardation and sorption tendency in the soil matrix (repacked soil columns), probably due to the straining and adsorption of antibiotics bound to manure particles in matrix pores. TKS and TSM models provided a valuable description of the BTCs and the fitted transport parameters strongly supported our findings. The presence of chicken manure and/or DOM may increase the leaching danger of SDZ and FFC in macroporous soils dominated by abundant preferential flow channels. Nevertheless, a similar condition in matrix soil may lead to substantial retardation and irreversible sorption of the antibiotics. This study provided a significant basis for the assessment of antibiotic leaching risks associated with manure-DOM under soil hydrological conditions.

**Supplementary Materials:** The following supporting information can be downloaded at: <https://www.mdpi.com/article/10.3390/agronomy12123228/s1>, Figure S1: Chemical structure of sulfadiazine (SDZ) and florfenicol (FFC); Figure S2: Experimental design of the antibiotic leaching experiment in the undisturbed field and laboratory-repacked soil columns Figure S3: Temporal water potential at 10 cm and 30 cm depth continuously measured in the open-orchard field (without lysimeter) during the four rainfall events (I–IV) observed. Figure S4: Breakthrough curves of Br compared with SDZ (a) and FFC (b) under various DOM treatment conditions fitted with two-site nonequilibrium adsorption model (TSM), and pairwise comparison of SDZ and FFC BTCs under control (c), DOM pre-coated (d), and cotransport (e) conditions fitted with two kinetic sites (TKS) model. Table S1: Mean values of antibiotics, selected physiochemical properties, EEM-PARAFAC components and DOC optical indices of lysimeter leachates under natural rainfall events (rainfall events 1–4). Table S2: Fitting parameters of two-site chemical nonequilibrium model coupled with Freundlich isotherm.

**Author Contributions:** Conceptualization, C.L. and X.T.; methodology, C.L., X.T. and L.A.G.; software, C.L., L.A.G. and X.L.; validation, C.L., L.A.G. and X.L.; formal analysis, L.A.G. and X.L.; investigation, L.A.G. and X.L.; resources, C.L., J.C., and X.T.; visualization, L.A.G. and X.L.; writing—original draft preparation, L.A.G.; writing—review and editing, L.A.G., J.C. and C.L.; supervision, C.L., J.C. and X.T.; project administration and funding acquisition C.L. and J.C. All authors have read and agreed to the published version of the manuscript.

**Funding:** This research was funded by the National Natural Science Foundation of China (41771521) and the Sichuan Science and Technology Program (2022YFS0500).

**Data Availability Statement:** The data that support the findings of this study are available upon reasonable request from the authors.

**Acknowledgments:** The authors appreciate the support from the CAS-TWAS President’s Fellowship for international PhD students.

**Conflicts of Interest:** The authors declare no conflict of interest.

## References

1. Van Boeckel, T.P.; Brower, C.; Gilbert, M.; Grenfell, B.T.; Levin, S.A. Global Trends in Antimicrobial Use in Food Animals. *Proc. Natl. Acad. Sci. USA* **2015**, *112*, 5649–5654. [[CrossRef](#)] [[PubMed](#)]
2. Krishnasamy, V.; Otte, J.; Silbergeld, E. Antimicrobial Use in Chinese Swine and Broiler Poultry Production. *Antimicrob. Resist. Infect. Control* **2015**, *4*, 17. [[CrossRef](#)] [[PubMed](#)]
3. Chen, Y.S.; Zhang, H.B.; Luo, Y.M.; Song, J. Occurrence and Assessment of Veterinary Antibiotics in Swine Manures: A Case Study in East China. *Chin. Sci. Bull.* **2012**, *57*, 606–614. [[CrossRef](#)]
4. Zhao, L.; Dong, Y.H.; Wang, H. Residues of Veterinary Antibiotics in Manures from Feedlot Livestock in Eight Provinces of China. *Sci. Total Environ.* **2010**, *408*, 1069–1075. [[CrossRef](#)] [[PubMed](#)]
5. Wu, Z. *Antibiotic Use and Antibiotic Resistance in Food-Producing Animals in China*; OECD Food, Agriculture and Fisheries Working Papers; OECD Publishing: Paris, France, 2019. [[CrossRef](#)]
6. Qiao, M.; Chen, W.; Su, J.; Zhang, B.; Zhang, C. Fate of Tetracyclines in Swine Manure of Three Selected Swine Farms in China. *J. Environ. Sci. China* **2012**, *24*, 1047–1052. [[CrossRef](#)]
7. Sarmah, A.K.; Meyer, M.T.; Boxall, A.B.A. A Global Perspective on the Use, Sales, Exposure Pathways, Occurrence, Fate and Effects of Veterinary Antibiotics (VAs) in the Environment. *Chemosphere* **2006**, *65*, 725–759. [[CrossRef](#)]
8. Jechalke, S.; Heuer, H.; Siemens, J.; Amelung, W.; Smalla, K. Fate and Effects of Veterinary Antibiotics in Soil. *Trends Microbiol.* **2014**, *22*, 536–545. [[CrossRef](#)]
9. Kay, P.; Blackwell, P.A.; Boxall, A.B.A. Fate of Veterinary Antibiotics in a Macroporous Tile Drained Clay Soil. *Environ. Toxicol. Chem.* **2004**, *23*, 1136–1144. [[CrossRef](#)]
10. Li, C.; Chen, J.; Wang, J.; Ma, Z.; Han, P.; Luan, Y.; Lu, A. Occurrence of Antibiotics in Soils and Manures from Greenhouse Vegetable Production Bases of Beijing, China and an Associated Risk Assessment. *Sci. Total Environ.* **2015**, *521–522*, 101–107. [[CrossRef](#)]
11. Yi, X.; Lin, C.; Ong, E.J.L.; Wang, M.; Zhou, Z. Occurrence and Distribution of Trace Levels of Antibiotics in Surface Waters and Soils Driven by Non-Point Source Pollution and Anthropogenic Pressure. *Chemosphere* **2019**, *216*, 213–223. [[CrossRef](#)]
12. Hu, X.; Zhou, Q.; Luo, Y. Occurrence and Source Analysis of Typical Veterinary Antibiotics in Manure, Soil, Vegetables and Groundwater from Organic Vegetable Bases, Northern China. *Environ. Pollut.* **2010**, *158*, 2992–2998. [[CrossRef](#)] [[PubMed](#)]
13. Chen, C.; Li, J.; Chen, P.; Ding, R.; Zhang, P.; Li, X. Occurrence of Antibiotics and Antibiotic Resistances in Soils from Wastewater Irrigation Areas in Beijing and Tianjin, China. *Environ. Pollut.* **2014**, *193*, 94–101. [[CrossRef](#)] [[PubMed](#)]

14. Joy, S.R.; Bartelt-Hunt, S.L.; Snow, D.D.; Gilley, J.E.; Woodbury, B.L.; Parker, D.B.; Marx, D.B.; Li, X. Fate and Transport of Antimicrobials and Antimicrobial Resistance Genes in Soil and Runoff Following Land Application of Swine Manure Slurry. *Environ. Sci. Technol.* **2013**, *47*, 12081–12088. [[CrossRef](#)] [[PubMed](#)]
15. Song, W.; Guo, M. Residual Veterinary Pharmaceuticals in Animal Manures and Their Environmental Behaviors in Soils. In *Applied Manure and Nutrient Chemistry for Sustainable Agriculture and Environment*; Springer: Dordrecht, The Netherlands, 2014; pp. 23–52. [[CrossRef](#)]
16. Chen, L.; Lang, H.; Liu, F.; Jin, S.; Yan, T. Presence of Antibiotics in Shallow Groundwater in the Northern and Southwestern Regions of China. *Groundwater* **2017**, *56*, 451–457. [[CrossRef](#)] [[PubMed](#)]
17. Danner, M.C.; Robertson, A.; Behrends, V.; Reiss, J. Antibiotic Pollution in Surface Fresh Waters: Occurrence and Effects. *Sci. Total Environ.* **2019**, *664*, 793–804. [[CrossRef](#)]
18. Sun, J.; Zeng, Q.; Tsang, D.C.W.; Zhu, L.Z.; Li, X.D. Antibiotics in the Agricultural Soils from the Yangtze River Delta, China. *Chemosphere* **2017**, *189*, 301–308. [[CrossRef](#)]
19. Tong, L.; Qin, L.; Xie, C.; Liu, H.; Wang, Y.; Guan, C. Chemosphere Distribution of Antibiotics in Alluvial Sediment near Animal Breeding Areas at the Jiangnan Plain, Central China. *Chemosphere* **2017**, *186*, 100–107. [[CrossRef](#)]
20. Kay, P.; Blackwell, P.A.; Boxall, A.B.A. A Lysimeter Experiment to Investigate the Leaching of Veterinary Antibiotics through a Clay Soil and Comparison with Field Data. *Environ. Pollut.* **2005**, *134*, 333–341. [[CrossRef](#)]
21. Pan, M.; Chu, L.M. Leaching Behavior of Veterinary Antibiotics in Animal Manure-Applied Soils. *Sci. Total Environ.* **2017**, *579*, 466–473. [[CrossRef](#)]
22. Fan, W.; Guo, T.; Gao, S.; Lu, Y.; Meng, Y.; Huo, M. Evolution of Dissolved Organic Matter during Artificial Groundwater Recharge with Effluent from Underutilized WWTP and the Resulting Facilitated Transport Effect. *Environ. Res.* **2021**, *193*, 110527. [[CrossRef](#)]
23. Xing, Y.; Chen, X.; Wagner, R.E.; Zhuang, J.; Chen, X. Coupled Effect of Colloids and Surface Chemical Heterogeneity on the Transport of Antibiotics in Porous Media. *Sci. Total Environ.* **2020**, *713*, 136644. [[CrossRef](#)] [[PubMed](#)]
24. Zhang, L.; Zhu, D.; Wang, H.; Hou, L.; Chen, W. Humic Acid-Mediated Transport of Tetracycline and Pyrene in Saturated Porous Media. *Environ. Toxicol. Chem.* **2012**, *31*, 534–541. [[CrossRef](#)] [[PubMed](#)]
25. Zhou, D.; Thiele-Bruhn, S.; Arenz-Leufen, M.G.; Jacques, D.; Lichtner, P.; Engelhardt, I. Impact of Manure-Related DOM on Sulfonamide Transport in Arable Soils. *J. Contam. Hydrol.* **2016**, *192*, 118–128. [[CrossRef](#)] [[PubMed](#)]
26. Zou, Y.; Zheng, W. Modeling Manure Colloid-Facilitated Transport of the Weakly Hydrophobic Antibiotic Florfenicol in Saturated Soil Columns. *Environ. Sci. Technol.* **2013**, *47*, 5185–5192. [[CrossRef](#)] [[PubMed](#)]
27. Boy-Roura, M.; Mas-Pla, J.; Petrovic, M.; Gros, M.; Soler, D.; Brusi, D.; Menció, A. Towards the Understanding of Antibiotic Occurrence and Transport in Groundwater: Findings from the Baix Fluvià Alluvial Aquifer (NE Catalonia, Spain). *Sci. Total Environ.* **2018**, *612*, 1387–1406. [[CrossRef](#)] [[PubMed](#)]
28. Burke, V.; Richter, D.; Greskowiak, J.; Mehrtens, A.; Schulz, L.; Massmann, G. Occurrence of Antibiotics in Surface and Groundwater of a Drinking Water Catchment Area in Germany. *Water Environ. Res.* **2016**, *88*, 652–659. [[CrossRef](#)]
29. Lei, K.; Han, X.; Fu, G.; Zhao, J.; Yang, L. Mechanism of Ofloxacin Fluorescence Quenching and Its Interaction with Sequentially Extracted Dissolved Organic Matter from Lake Sediment of Dianchi, China. *Environ. Monit. Assess.* **2014**, *186*, 8857–8864. [[CrossRef](#)]
30. Bai, L.; Zhao, Z.; Wang, C.; Wang, C.; Liu, X.; Jiang, H. Multi-Spectroscopic Investigation on the Complexation of Tetracycline with Dissolved Organic Matter Derived from Algae and Macrophyte. *Chemosphere* **2017**, *187*, 421–429. [[CrossRef](#)]
31. Lou, Y.; Ye, Z.L.; Chen, S.; Wei, Q.; Zhang, J.; Ye, X. Influences of Dissolved Organic Matters on Tetracyclines Transport in the Process of Struvite Recovery from Swine Wastewater. *Water Res.* **2018**, *134*, 311–326. [[CrossRef](#)]
32. Xu, J.; Yu, H.Q.; Sheng, G.P. Kinetics and Thermodynamics of Interaction between Sulfonamide Antibiotics and Humic Acids: Surface Plasmon Resonance and Isothermal Titration Microcalorimetry Analysis. *J. Hazard. Mater.* **2016**, *302*, 262–266. [[CrossRef](#)]
33. Ahmed, A.A.; Thiele-Bruhn, S.; Aziz, S.G.; Hilal, R.H.; Elroby, S.A.; Al-Youbi, A.O.; Leinweber, P.; Kühn, O. Interaction of Polar and Nonpolar Organic Pollutants with Soil Organic Matter: Sorption Experiments and Molecular Dynamics Simulation. *Sci. Total Environ.* **2015**, *508*, 276–287. [[CrossRef](#)] [[PubMed](#)]
34. Xiao, Y.H.; Huang, Q.H.; Vähätalo, A.V.; Li, F.P.; Chen, L. Effects of Dissolved Organic Matter from a Eutrophic Lake on the Freely Dissolved Concentrations of Emerging Organic Contaminants. *Environ. Toxicol. Chem.* **2014**, *33*, 1739–1746. [[CrossRef](#)] [[PubMed](#)]
35. Yang, F.; Zhang, Q.; Jian, H.; Wang, C.; Xing, B.; Sun, H.; Hao, Y. Effect of Biochar-Derived Dissolved Organic Matter on Adsorption of Sulfamethoxazole and Chloramphenicol. *J. Hazard. Mater.* **2020**, *396*, 122598. [[CrossRef](#)] [[PubMed](#)]
36. Zhao, X.; Hu, Z.; Yang, X.; Cai, X.; Wang, Z.; Xie, X. Noncovalent Interactions between Fluoroquinolone Antibiotics with Dissolved Organic Matter: A <sup>1</sup>H NMR Binding Site Study and Multi-Spectroscopic Methods. *Environ. Pollut.* **2019**, *248*, 815–822. [[CrossRef](#)]
37. Zhang, W.; Tang, X.Y.; Weisbrod, N.; Zhao, P.; Reid, B.J. A Coupled Field Study of Subsurface Fracture Flow and Colloid Transport. *J. Hydrol.* **2015**, *524*, 476–488. [[CrossRef](#)]
38. Zhao, P.; Tang, X.; Zhao, P.; Wang, C.; Tang, J. Identifying the Water Source for Subsurface Flow with Deuterium and Oxygen-18 Isotopes of Soil Water Collected from Tension Lysimeters and Cores. *J. Hydrol.* **2013**, *503*, 1–10. [[CrossRef](#)]
39. Wang, H.L. *Study on Soil Hydraulic Parameters of Forest Land and Sloping Farmland in the Hilly Area of Central Sichuan Basin*; Northwest A&F University: Yangling, China, 2013.

40. Haham, H.; Oren, A.; Chefetz, B. Insight into the Role of Dissolved Organic Matter in Sorption of Sulfapyridine by Semiarid Soils. *Environ. Sci. Technol.* **2012**, *46*, 11870–11877. [[CrossRef](#)]
41. Stedmon, C.A.; Bro, R. Characterizing Dissolved Organic Matter Fluorescence with Parallel Factor Analysis: A Tutorial. *Limnol. Oceanogr. Methods* **2008**, *6*, 572–579. [[CrossRef](#)]
42. Cory, R.M.; McKnight, D.M. Fluorescence Spectroscopy Reveals Ubiquitous Presence of Oxidized and Reduced Quinones in Dissolved Organic Matter. *Environ. Sci. Technol.* **2005**, *39*, 8142–8149. [[CrossRef](#)]
43. Ohno, T. Fluorescence Inner-Filtering Correction for Determining the Humification Index of Dissolved Organic Matter. *Environ. Sci. Technol.* **2002**, *36*, 742–746. [[CrossRef](#)]
44. Šimunek, J.; Sejna, M.; Saito, H.; Genuchten, M.T.V. *The HYDRUS-1D Software Package for Simulating the One-Dimensional Movement of Water, Heat, and Multiple Solutes in Variably-Saturated Media*; University of California Riverside: Riverside, CA, USA, 2008.
45. Selim, H.M.; Davidson, J.M.; Mansell, R.S. Evaluation of a Two-Site Adsorption–Desorption Model for Describing Solute Transport in Soil. In Proceedings of the Conference on Applications of Continuous System Simulation Languages, Washington, DC, USA, 12–14 July 1976; pp. 444–448.
46. van Genuchten, M.T.; Wagenet, R.J. Two-Site/Two-Region Models for Pesticide Transport and Degradation: Theoretical Development and Analytical Solutions. *Soil Sci. Soc. Am. J.* **1989**, *53*, 1303–1310. [[CrossRef](#)]
47. Šimunek, J.; Jacques, D.; Langergraber, G.; Bradford, S.A.; Šejna, M.; Van Genuchten, M.T. Numerical Modeling of Contaminant Transport Using HYDRUS and Its Specialized Modules. *J. Indian Inst. Sci.* **2013**, *93*, 265–284.
48. Gbadegesin, L.A.; Tang, X.; Liu, C.; Cheng, J. Transport of Veterinary Antibiotics in Farmland Soil: Effects of Dissolved Organic Matter. *Int. J. Environ. Res. Public Health* **2022**, *19*, 1702. [[CrossRef](#)] [[PubMed](#)]
49. Zhang, W.; Tang, X.Y.; Xian, Q.S.; Weisbrod, N.; Yang, J.E.; Wang, H.L. A Field Study of Colloid Transport in Surface and Subsurface Flows. *J. Hydrol.* **2016**, *542*, 101–114. [[CrossRef](#)]
50. Wang, N.; Guo, X.; Xu, J.; Hao, L.; Kong, D.; Gao, S. Sorption and Transport of Five Sulfonamide Antibiotics in Agricultural Soil and Soil–Manure Systems. *J. Environ. Sci. Health Part B Pestic. Food Contam. Agric. Wastes* **2015**, *50*, 23–33. [[CrossRef](#)]
51. Engelhardt, I.; Sittig, S.; Šimunek, J.; Groeneweg, J.; Pütz, T.; Vereecken, H. Fate of the Antibiotic Sulfadiazine in Natural Soils: Experimental and Numerical Investigations. *J. Contam. Hydrol.* **2015**, *177–178*, 30–42. [[CrossRef](#)]
52. Sukul, P.; Lamshöft, M.; Zühlke, S.; Spittler, M. Sorption and Desorption of Sulfadiazine in Soil and Soil-Manure Systems. *Chemosphere* **2008**, *73*, 1344–1350. [[CrossRef](#)]
53. Conde-Cid, M.; Fernández-Calviño, D.; Fernández-Sanjurjo, M.J.; Núñez-Delgado, A.; Álvarez-Rodríguez, E.; Arias-Estévez, M. Adsorption/Desorption and Transport of Sulfadiazine, Sulfachloropyridazine, and Sulfamethazine, in Acid Agricultural Soils. *Chemosphere* **2019**, *234*, 978–986. [[CrossRef](#)]
54. Tang, X.; Liu, C.; Luo, F.; Li, S.; Yang, H. Effects of Colloidal Manure DOM on the Transport of Antibiotics in Calcareous Soils. In Proceedings of the EGU General Assembly 2021, Online, 19–30 April 2021. [[CrossRef](#)]
55. Gao, J.; Shi, Z.; Gao, J.; Wu, H.; Lv, J. Fluorescent Characteristics of Dissolved Organic Matter Released from Biochar and Paddy Soil Incorporated with Biochar. *RSC Adv.* **2020**, *10*, 5785–5793. [[CrossRef](#)]
56. Liu, C.; Li, Z.; Berhe, A.A.; Xiao, H.; Liu, L.; Wang, D.; Peng, H.; Zeng, G. Characterizing Dissolved Organic Matter in Eroded Sediments from a Loess Hilly Catchment Using Fluorescence EEM-PARAFAC and UV–Visible Absorption: Insights from Source Identification and Carbon Cycling. *Geoderma* **2019**, *334*, 37–48. [[CrossRef](#)]
57. Xian, Q.; Li, P.; Liu, C.; Cui, J.; Guan, Z.; Tang, X. Concentration and Spectroscopic Characteristics of DOM in Surface Runoff and Fracture Flow in a Cropland Plot of a Loamy Soil. *Sci. Total Environ.* **2018**, *622–623*, 385–393. [[CrossRef](#)] [[PubMed](#)]
58. Zhang, Y.; Zhang, B.; He, Y.; Lev, O.; Yu, G.; Shen, G.; Hu, S. DOM as an Indicator of Occurrence and Risks of Antibiotics in a City-River-Reservoir System with Multiple Pollution Sources. *Sci. Total Environ.* **2019**, *686*, 276–289. [[CrossRef](#)] [[PubMed](#)]
59. Mu, G.; Ji, M.; Li, S. Evaluation of CDOM Sources and Their Links with Antibiotics in the Rivers Dividing China and North Korea Using Fluorescence Spectroscopy. *Environ. Sci. Pollut. Res.* **2018**, *25*, 27545–27560. [[CrossRef](#)] [[PubMed](#)]
60. Wehrhan, A.; Kasteel, R.; Šimunek, J.; Groeneweg, J.; Vereecken, H. Transport of Sulfadiazine in Soil Columns—Experiments and Modelling Approaches. *J. Contam. Hydrol.* **2007**, *89*, 107–135. [[CrossRef](#)]
61. Unold, M.; Šimunek, J.; Kasteel, R.; Groeneweg, J.; Vereecken, H. Transport of Manure-Based Applied Sulfadiazine and Its Main Transformation Products in Soil Columns. *Vadose Zone J.* **2009**, *8*, 677–689. [[CrossRef](#)]